Conceptual design of an autonomous single-container vessel

Hompes, J.T.; Hendriks, P.M.S.; Cuijpers, J.P.T.; Wolterbeek, T.J.F.; Sougé, W.D.; Nishiki, Yoshinari ; Garofano, V.; Jovanova, J.

DOI
10.3389/ffutr.2024.1443271

Publication date
2024

Document Version
Final published version

Published in
Frontiers in Future Transportation

frontiers | Frontiers in Future Transportation

TYPE Original Research
PUBLISHED 11 October 2024
DOI 10.3389/ffutr.2024.1443271

OPEN ACCESS

EDITED BY
Luca Braidotti,
University of Trieste, Italy

REVIEWED BY
Andrea Gallo,
Ca' Foscari University of Venice, Italy
Samuele Utzeri,
University of Trieste, Italy

*CORRESPONDENCE
Yoshinari Nishiki,
inari@irational.org

†PRESENT ADDRESS
Yoshinari Nishiki,
Nara Institute of Science and Technology,
Nara, Japan

RECEIVED 03 June 2024
ACCEPTED 23 September 2024
PUBLISHED 11 October 2024

CITATION
Hompes JT, Sebastiaan Hendriks PM, Tjalling Cuijpers JP, Frederik Wolterbeek TJ, Sougé WD, Nishiki Y, Garofano V and Jovanova J (2024) Conceptual design of an autonomous single-container vessel. *Front. Future Transp.* 5:1443271. doi: 10.3389/ffutr.2024.1443271

Conceptual design of an autonomous single-container vessel

Jouke Thomas Hompes[1], Pieter Max Sebastiaan Hendriks[1], Jelle Paul Tjalling Cuijpers[1], Ties Johannes Frederik Wolterbeek[1], Wouter Dick Sougé[1], Yoshinari Nishiki[2*†], Vittorio Garofano[1] and Jovana Jovanova[1]

[1]Faculty of Mechanical Engineering, Delft University of Technology, Delft, Netherlands, [2]Technology of Future Utopia (TOFU), Rotterdam, Netherlands

The growth of maritime shipping is leading to the creation of larger vessels. However, this expansion in size brings with it several challenges, including the development of maritime infrastructure, the potential for growth in third-world countries, and the emission of greenhouse gases. In response to these challenges, this research explores the feasibility of designing an autonomous ship capable of transporting a single standardized 40 ft. container overseas using mainly passive propulsion methods. Using advanced design tools, including CAD software and CFD simulations, as well as conducting a comprehensive analysis of relevant literature, the designs for a hull and sails were developed, and an overview of the potential active control systems required for autonomous operation was provided. The study also performed an initial analysis of strength, stability, and velocity to validate the design choices. The ship proves to adhere to the basic strength and stability requirements while reaching its maximum hull velocity at certain wind speeds. The results of the study indicate that it is possible to design and manufacture a mainly passively propelled ship capable of transporting a 40 ft. standardized container overseas and rethink the logistics at scale.

KEYWORDS

maritime shipping, small-scale, sustainable, passive propulsion, autonomous, design

Introduction

International shipping is frequently referred to as the backbone of global trade and is therefore subject to continuous improvement. As technology has advanced, the size of cargo vessels in overseas shipping has increased, resulting in lower costs per container. However, this progress has resulted in several drawbacks with global consequences. First, the increase in vessel sizes necessitates the expansion of existing maritime transport infrastructure, which many underdeveloped countries lack the resources to achieve, hindering their ability to benefit from economies of scale (Sirimanne and Hoffmann, 2020). Secondly, the expansion of infrastructure is not always feasible, leading to bigger vessels navigating size-constrained waterways, increasing the risk of world-impacting complications (ITF, 2015; Russon, 2021). Finally, the maritime transport sector is responsible for the emission of 940 million tonnes of CO2 annually, accounting for 2.5% of worldwide greenhouse gas emissions. While other transport sectors are pursuing more sustainable alternatives, if the maritime transport sector continues its "business as usual" scenario, its emissions could increase by 50%–250% by 2050 as listed on the website of the European Commission as of 29 June 2021.

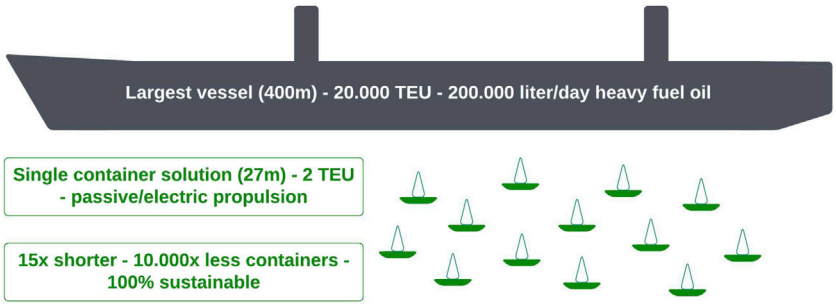

FIGURE 1
Dimensional comparison of largest container vessel and potential single 40 ft. container solution in fleet.

When questioning the current trend in maritime freight, it is tempting to try a reversed mindset and explore the miniaturization of vessels instead of the "ever growing" mentality as visualized in Figure 1. Jumping to the extreme, what role could a single container vessel fulfil? Such a small vehicle could benefit from sustainability innovations and sail with more ecological responsibility and could possibly even be deployed autonomously. Above all, underdeveloped countries and pressurized infrastructure would benefit the most. To gain a more nuanced answer to this question, the goal of this research is to explore the viability of the design of autonomous single container vessel to enable zero-emission, autonomous, wind propelled, overseas transport of a standardized 40 ft. container.

Rødseth and Nordahl (2017) have characterized autonomous maritime vehicles into two main subcategories: unmanned underwater vehicles and autonomous surface vehicles. With the latter being the main topic of this paper, autonomous surface vessels have again been subcategorized into unmanned surface vehicles (USVs) and Maritime autonomous surface ships (MASS). USV's main current purpose is in marine research and in the military sector, as they are often characterized as being small, fast and deployable in a vast range of environments (Heo et al., 2017). The United States deploys USVs for counter-terrorism operations, automatic submarine tracking, complete mission execution, and surveillance. The Israeli defense uses its USVs, KATANA, PROTECTOR and Silver Marlin, for port security, coastal reconnaissance, minesweeping and enemy submarine detection. Lastly, Singapore and France deploy USVs for maritime block operations and rescue missions. Practically all of these USVs are designed to excel in operation capabilities in contrast to a high level of sustainability. MASS ships on the other hand are usually large and designed for civil purposes like transporting goods or people. In a pilot project in Norway, the container ship Yara Birkeland (80 m) is expected to convey fertilizer autonomously with zero emissions from a manufacturing plant to an export port which is expected to be operational in 2024 (Negenborn et al., 2023). In China, a 120-m electric container ship called Zhi Wei has demonstrated to shuttle remotely and sometimes autonomously between two ports in Shandong province. Judging from these examples, small-scale autonomous designs for civil purposes and specifically featuring passive propulsion remain scarce in literature. Despite existing research on autonomous passive propulsion, research has currently primarily been centered around improving and automating existing large-scale maritime shipping systems or on sustainable autonomous movement at sea for mapping and monitoring purposes like Saildrone and SailBuoy (Santos and Gonçalves, 2020; Anthierens et al., 2013; King, 2017; Gentemann et al., 2020; Tretow, 2017; Ghani et al., 2014). No attempt has been made to leverage advances on autonomous maritime travel to create a small-scale transport alternative in a sustainable fashion. This research aims to initiate a movement towards sustainable small-scale shipping research by providing a first design in the field of sustainable, small-scale, autonomous maritime transport.

Although creative solutions are rising, substitution of the current large-scale maritime transport system currently might seem too utopian, scenarios exist where a sustainable autonomous single container vessel could act as a complementary system (Weber, Wiek, and Lang, 2019). Archipelagos, groups of islands clustered together in a large body of water like oceans or seas, are found around the world. Due to the commonly small size of the individual islands, accessibility remains a challenge. For instance, in the Indonesian archipelago, challenges in integrating transport systems persist, which are necessary for economic improvement (Ralahalu and Jinca, 2013). Similarly, in the Finnish rural archipelago, island populations are in decline due to accessibility issues, with a heavy reliance on ferries for goods and transport, where a sustainable autonomous single container vessel could provide continuous supply (Makkonen, Salonen and Kajander, 2013). In the Canary Islands, the lack of infrastructure in many areas hampers sustainability efforts, where the sustainable autonomous single container vessel could offer a viable means to reach remote parts effectively (Castanho et al., 2020). Additionally, the Azores face challenges such as limited resources, restricted land, mass tourism, and connectivity barriers, making them crucial for examining territorial governance and sustainable development (Castanho et al., 2021). Due to the mere requirement for small and potentially fully autonomous ports, the sustainable autonomous single container vessel could provide a significant contribution to the limitations that archipelagos bear. The introduction of this new approach to connectivity could serve as a valuable inspiration to the massively scaled global maritime trade of today in terms of sustainability and autonomy.

Ultimately, this paper will be centered around the physical aspect of the design challenge proposed by the goal of the research. A hull and sail mechanism will be designed and integrated to ensure optimal compatibility. As this study is

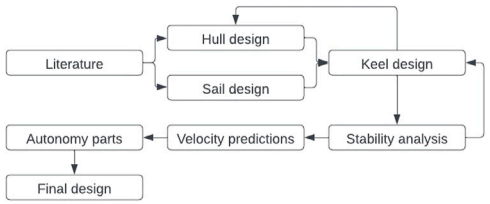

FIGURE 2
Design methodology.

centered on conceptual design, it includes essential calculations to demonstrate the basic feasibility of the proposed design, while more detailed calculations are intentionally excluded from its scope. Since this study concerns an autonomous ship, a brief discussion on active control systems for autonomy will be addressed, including necessary adjustments for implementation. In this paper, the main propulsion at sea is assumed to be passive with an efficient way of actively steering.

Design method

The main goal of this research is to make an integrated design. Therefore, an elaboration on three design aspects has been made: hull, sail, and components for autonomy. The design methodology is inspired by the 'The Basic Design Cycle' (Boeijen and Daalhuizen, 2014) and is graphically represented in Figure 2.

Hull design

The initial step in the process is to set up the requirements of the design. In the formation of the requirements, knowledge about existing ships and vessels is considered. The requirements are stated below.

(1) The vessel must be able to house and transport one full-size 40 ft. standardized container.
(2) The ship must have a precisely designed depth draft as a result of the mass of the ship and the keel.
(3) A cargo hatch must be incorporated into the design to accommodate the loading and unloading capabilities of the container.
(4) The construction of the hull should be designed to withstand the various conditions at sea.
(5) The hull design shall incorporate the capability to withstand capsize and shall be capable of self- righting from any possible orientation.
(6) The hull structure must be rigid enough to carry its own weight during hoisting operations and rough sea conditions.
(7) The ship must contain different air pockets in the hull to stay afloat when punctured locally.
(8) The design of the hull should prioritize the use of straight plates over shaped sheets to enhance manufacturability.

The study utilized analytical models to conduct initial qualitative simulations of laminar flow around an object in 2D. Subsequently, CAD software was used to create a 3D design of a hull. The 3D design was used to perform initial flow simulations in the computational domain of the software to obtain quantitative analysis. The shapes of the tip and rear were iteratively adjusted and simulated, aiming to find a shape with low drag force and straight plate work, under the assumption of the ship only operating in laminar flow conditions. The results of these Computational Fluid Dynamics (CFD) simulations provided valuable insights into the properties of the designed shapes and a function relating the hull resistance F_{hull} to the vessel velocity V_B was established. The final hull design was derived from the best performing tip and rear. The maximum hull speed (v_m) was calculated using Formula 1, where L_w represents the length of the waterline (Fossati, 2009).

$$v_m = 1.34\sqrt{L_w} \tag{1}$$

The next design validation approach used was a static strength analysis, with dynamic strength analysis assumed to be beyond the scope of this study. The study focused on the longitudinal and transverse, or inward, strength loads as the primary mechanisms in ships as described in (Keuning, 2015). The local strength loads were not considered in this analysis. The hull was simplified as a U-shaped beam for the purpose of conducting a strength analysis of the steel plating, taking into account a fully loaded container (29 tons) and an approximation of the sail mass. The hull was assumed to be constructed from 4 mm thick steel. Bending moment lines were constructed for the conditions of hogging and sagging (Okumoto et al., 2009), based on classic beam theory. Using Equations 2, 3, respectively stress (σ) and second moment of inertia around the centroid axis (I_x) were calculated. In Equation 2, y indicates the height in the hull.

$$\sigma = \frac{-M \cdot y}{I_x} \tag{2}$$

$$I_x = \iint_R y^2 dx dy \tag{3}$$

For the transverse loads, the stress and displacement of the plating at the bottom of the hull as a result of hydrostatic pressure were calculated with Equation 4 (Keuning, 2015) and empirical formulae Equations 5, 6 (Engineers Edge, 2021). Here, a fully submerged situation was assumed, to simulate an upper boundary situation.

$$p = p_0 + \rho g d \tag{4}$$

$$\sigma_m = \frac{pa^2}{2t^2\left(0.623\left(\frac{a}{b}\right)^6 + 1\right)} \tag{5}$$

$$y_m = \frac{0.0284pa^4}{Et^3\left(1.056\left(\frac{a}{b}\right)^5 + 1\right)} \tag{6}$$

Equation 4 describes the pressure at depth, Equation 5 the stress in a plate and Equation 6 the displacement of a plate. p is the relevant hydro static pressure (Pa), and the short side of the plate (m), b the long side of the plate (m), t the thickness (m), and E the assumed modulus of elasticity (210 GPa).

After conducting more analyses on the loads and hydro-static pressure that the hull needs to withstand, an internal reinforcement plan was made. This aimed at designing a hull with the capacity of

withstanding pressure, buckling forces, torsional forces and bending forces in longitudinal, and transverse directions. It also included sections for the air pockets mentioned in requirement 7.

At this point, a seemingly accurate estimation of the reinforcement, hull, and sail masses can be made to make an iterative step to verify the strength of the hull again using Equations 2, 3.

Based on the results of the previous stability analysis, the keel design was optimized to meet the desired level of stability by controlling the draft depth and centre of gravity. The centre of mass, sail dimensions and weight were considered due to their impact on the centre of mass. Literature from Fossati (2009) was utilized to estimate the required surface area of the keel, and the findings were incorporated into the 3D CAD design. With the keel integrated into the CAD design, an iterative step was made to ensure the integrity of the hull structure as visualized in Figure 2. The center of buoyancy was determined using the CAD model. The locations of the Centre Of Mass (G), Centre Of Buoyancy (COB), and the intersection of the vertical line through the COB and the line through the G, known as Metacentre point M, were graphically determined for different situations to assess the stability of the design according to (Keuning, 2015). Again, an iterative step was taken to refine the keel aiming at stability (Figure 2). Finally, the hull was adjusted to house the masts and a cargo hatch was implemented.

Sail design

The design process of the sail comprised of multiple stages. Initial requirements were established based on existing sail knowledge, with the aim of achieving a target speed of 5 km/h, given the global average wind speed over the ocean, measured as 6.64 m/s (Archer and Jacobson, 2005). The requirements were established as follows:

(1) The sail creates enough thrust at average conditions to reach the target speed, while the vessel remains stable under the resulting centre of mass.
(2) The sail is easily and autonomously trimmable, while low energy consuming.
(3) The sail should be lightweight to reduce the load on the mast and lower the centre of mass of the vessel.
(4) The sail and mast are corrosion resistant in a saltwater environment.
(5) The sail and mast have a structural rigidity to prevent structural loads or fatigue to cause plastic deformation and do not deform in rough weather conditions.

As one of the set requirements is that the sail needs to be low energy consuming, conventional soft sails are overlooked, since they require much attention, and thus energy, for their optimal position. The literature study only considered hard wing sail profiles and compared their lift-to-drag ratio for various Reynolds numbers.

The following steps were followed to determine the suit- able sail area for the vessel: a cruising velocity was selected to determine the hull friction force at that speed, the necessary thrust force required from the sail to reach that velocity was calculated, the required sail area was determined to generate the necessary thrust force using Equations 7–14 which are derived from Keuning (2015).

$$F_D = \frac{1}{2}\rho_a C_D A_S V_A^2 \tag{7}$$

$$F_L = \frac{1}{2}\rho_a C_L A_S V_A^2 \tag{8}$$

In Equations 7, 8, ρ_a represents the density of air, C_D and C_L respectively the drag and lift coefficients of the wing sail, As the wing sail area, and V_A the apparent wind speed. The direction of the apparent wind is calculated using the speed of the boat V_B and the true wind V_T, and the Pythagorean theorem. The generated lift force is perpendicular to the apparent wind direction. The generated drag force is parallel to the apparent wind direction. The apparent wind can be characterized as 'the wind felt by the boat as it moves through the air' and was calculated using Equation 9.

$$V_A = \sqrt{V_{B_x}^2 + \left(V_T + V_{B_y}\right)^2} \tag{9}$$

The apparent wind is then split into its vertical and horizontal components to determine the angle at which the apparent wind differs from the true wind (θ_{VA}) to determine the useful components of the generated lift and drag forces.

$$\theta_{V_A} = tan^{-1}\left(\left|V_{A_x}\right| / \left|V_{A_y}\right|\right) \tag{10}$$

θ_{VA} is used together with θ_{boat}, which is the angle of the boat's direction relative to the direction where the true wind comes from, to calculate the angle φ. Using the angle φ, the components parallel and perpendicular to the boat can be calculated, and thus the thrust and heeling forces.

$$\phi = \frac{\pi}{2} - \theta_{boat} + \theta_{V_A} \tag{11}$$

Leading to the formulae for the parallel lift and drag forces relative to the boat, Equations 12, 13. Equation 14 represents the total generated thrust force in the direction parallel to the movement of the vessel.

$$F_{D_x} = F_D \cdot sin\left(\phi + \theta_{V_A}\right) \tag{12}$$

$$F_{L_x} = F_L \cdot sin\left(\frac{\pi}{2} - \phi - \theta_{V_A}\right) \tag{13}$$

$$F_{x_{res}} = F_{D_x} + F_{L_x} \tag{14}$$

With these formulae several iterations have been done, to evaluate the thrust at different values for θ_{boat}, for different sail areas. A sail area capable of generating enough trust to reach the hull speed is chosen. This method is further utilized to make velocity predictions at different wind speeds and various θ_{boat}. To reach more accurate estimations of the velocity of the vessel at different wind speeds and angles of attack, Equations 7–14 are used in a numerical manner. The algorithm to calculate the velocity of the vessel requires the velocity itself in Equation 9. Therefore first, the velocity of the boat is estimated and the forward thrust F_{Lx} needed for this velocity is calculated. Assuming an equilibrium state of the vessel while sailing, the forward thrust must be equal to the vessel's hull resistance (F_{hull}) as in Equation 15 and is thus approached in this numerical algorithm.

$$F_{x_{res}} = F_{hull} \tag{15}$$

According to the vessel velocity vs. hull resistance function found in the hull design, the corresponding hull speed at the found forward thrust level is used as the new vessel velocity to determine the forward thrust in the next iteration. Iterations are performed until the error between forward thrust and hull resistance is insignificant, i.e., Equation 16 is met. The resulting boat velocity (V_B) is determined for different wind speeds and angles of attack and is graphically presented.

$$F_{x_{res}} - F_{hull} < 0.01 \tag{16}$$

To conclude if the sail design meets the set requirements, a 3D CAD model is made of the sail to use CFD to see if the tip and bottom vortex forces are minimized. To prevent a moment caused by the sail about the mast, the centre of mass of the sail is carefully positioned by adjusting the shape and dimensions of the sail and integrating a counterweight. The shape of the sail and the aerofoil profile also determine the point where the resulting force of the wind acts upon. This point is called the Centre Of Effort (COE). For the trimming of the sail, literature studies were used to determine an energy-efficient way of turning the sail into the optimal angle of attack.

To decide what material would be suitable for the sails to meet the requirements, GRANTA EduPack was used to find the best materials for a lightweight sail in a rough saltwater environment (ANSYSInc, 2023). For the sails a high Young's modulus and low density is desired and for the masts high tensile and fatigue strength.

In the design of the mast, classic beam theory was employed. The inner and outer diameters of the mast were determined using this method, leading to the calculation of stress using Equation 2. To ensure that the stress does not exceed the allowable fatigue strength, a Factor Of Safety (FOS) of three was applied. This safety margin was chosen due to the use of a reliable material under challenging and harsh environmental conditions (Fossati, 2009). The moment of inertia was calculated using Equation 17.

$$I = \frac{\pi}{64}\left(D_{large}^4 - d_{small}^4\right) \tag{17}$$

The Free Body Diagram (FBD) of the mast is used to calculate the maximum bending moment. The fatigue strength is assumed to be one third of the tensile strength of the material which is found via the GRANTA database (Zhang et al., 2020). For the beam holding the steering flap, the dimensions were calculated using classic beam theory as well. However, when calculating the maximum bending moment instead of using the forces generated by the wind, the mass of the flap (250 kg) was used in the FBD.

Design of a control framework for autonomous navigation

Once proven that the ship can sail at any wind speed in any direction, in this section autonomous navigation capabilities are addressed. A ship is considered to be autonomous when: "The situation is perceived and assessed and a decision on which action to take is made without any intervention by human beings" (Blanke et al., 2017), To meet this definition, the following three main requirements should be achieved:

(1) Autonomously navigating while avoiding static and dynamic obstacles.
(2) Identify other ships and obstacles in the environment.
(3) Self-monitoring capabilities for safe sailing condition.

The concept of autonomous ship navigation has taken a forefront position in the last years, driven by the technological development of the Guidance-Navigation-Control (GNC) framework. This framework is pivotal in transforming traditional maritime operations into intelligent, autonomous systems capable of navigating in unpredictable marine environment.

The GNC framework consists of three integral components, each fulfilling a distinct but inter-dependent role. The Guidance system is responsible of the strategic navigation decision, responsible for path planning. It leverages global positioning data and environmental inputs to calculate an optimal path, considering maritime traffic, weather conditions, and regulated no-sail zones. This constant pathfinding operation is crucial for efficient and safe navigation.

The Navigation subsystem serves as the vessel's eyes, equipped with sophisticated sensors such as radar, LiDAR, dedicated stereo-camera technology, and the Automatic Identification System (AIS). These technologies work together to detect, classify, and understand various objects and potential obstacles within the ship's environment. The precision and reliability of this system are very important for real-time decision-making and situational awareness.

Complementing these is the Control subsystem, the execution system of the GNC framework (Figure 3). Utilizing advanced control algorithms, based on error minimization and vessel model dynamics, this system ensures that the vessel follows the planned path. It dynamically adjusts the course in response to navigation inputs, ensuring obstacle avoidance and maintaining the vessel's operational integrity.

Based on the foundational concept illustrated, the next sections delves into a detailed overview of the various sensors utilized in the autonomous navigation system design, This will complemented by an in-depth discussion of the network data exchange mechanism, providing a complete description of how these components synergically works to ensure efficient and reliable autonomous operation.

Final design

In this section, all results will be presented for the hull design, sail design, and components for autonomy.

Hull design

The 2D laminar flow simulations revealed that a box shape generates a significant low-pressure zone at the rear and a high-pressure zone at the front. Streamlining the front and rear of the object resulted in changes to the boundary layer behaviour. These observations were applied in the 3D flow simulations, where it was

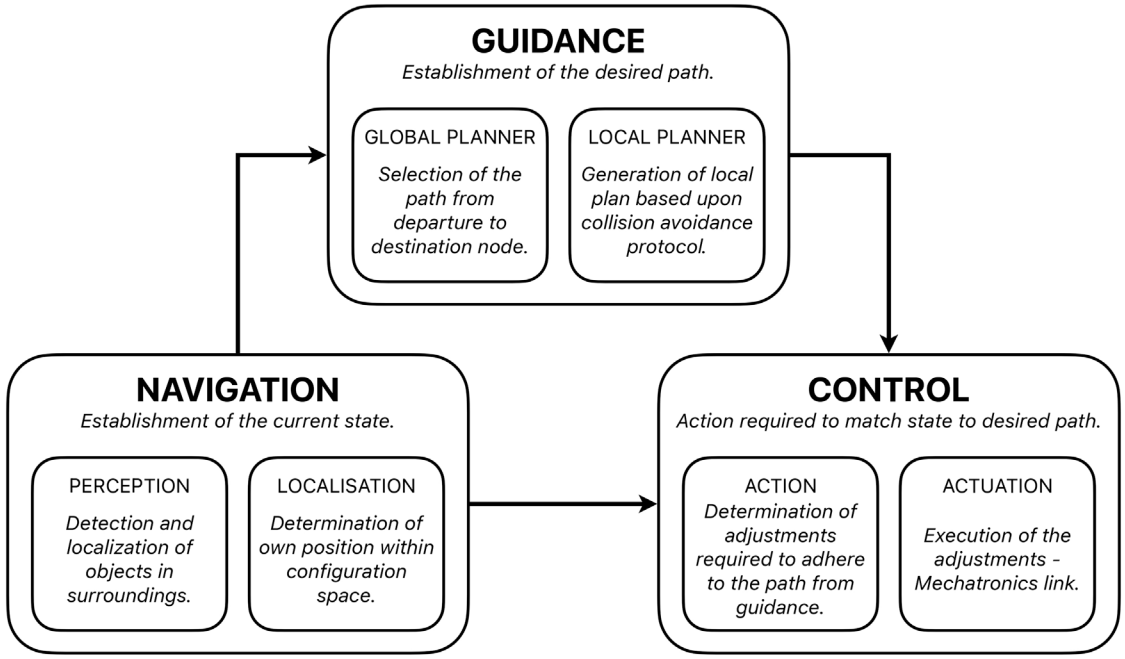

FIGURE 3
The Guidance, Navigation and Control Framework.

TABLE 1 Final (bare) hull flow specifications.

Parameter	Unit	Quantity
Nominal velocity	[m/s]	3.3
Maximum pressure	[kPa]	141
Friction force	[kN]	2.02
Normal force	[kN]	3.52
Total force	[kN]	5.54

TABLE 2 Results longitudinal loads.

Parameter	Unit	Quantity
Second moment of inertia (I_x)	[m^4]	0.0382
Maximum stress sagging	[MPa]	47.8
Maximum stress hogging	[MPa]	27.2

noted that sharp edges caused vortexes and elevated local flow speeds. The CFD analysis of the final design, combining the tip and rear, is presented in Table 1. It is important to note that these results are based on simulations of the bare hull without considering the integration of a keel, rudder, or potential propellers. A main propeller and a bow truster are required to manoeuvre the ship in ports, to assist in heavy weather and to use in emergency situations. The maximum hull speed resulting from Equation 1 resulted in 6.8 m/s.

The results of the longitudinal strength loads and transverse strength are shown in Table 2.

TABLE 3 Results transverse loads.

Parameter	Unit	Quantity
Pressure	[bar]	1.31
Maximum stress ($\sigma|m$)	[kPa]	21.0
Maximum displacement ($y|m$)	[mm]	7.0

The results of the transverse load analysis are stated in Table 3.

The chosen reinforcements are as follows. A steel torsion box spanning 25 m over the length of the ship, with a hollow rectangular cross-section, welded to the inside of the horizontal plate work of the hull (Figure 4 part 19; Figure 5). Also, steel transverse plates are inserted along the entire length of the hull (Figure 4 part 17; Figure 6), spacing 40 cm between each other, leaving a void for the container to be housed in. Most of the transverse plates in the tip and the rear are hollow, with one in every three or four plates being solid. Also, three longitudinal stiffeners are positioned symmetrically along the entire length on the bottom of the hull (Figure 4 part 13; Figure 7). The integration of the torsion box, longitudinal stiffeners and transverse plates are assumed to relax the outer structure of the ship sufficiently, and a consecutive torsion analysis and shear correction are assumed to lie outside the scope of the study. In the container compartment, two beams are used to integrate the corner locks of the container.

The results of the corrected longitudinal loads after integration of sails and keel are shown in Table 4.

The waterline and stability analysis required a 30-ton keel, as depicted in Figure 4 part 9. The keel ensured that the hull, excluding keel, was submerged between 23% and 33%. The combined weight of the hull, reinforcements, and sails was approximately 90 tons, with

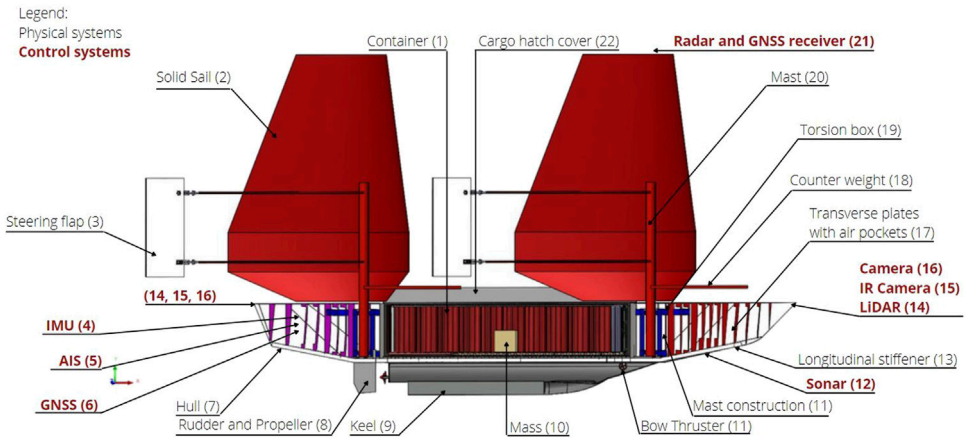

FIGURE 4
Cut out overview of complete design.

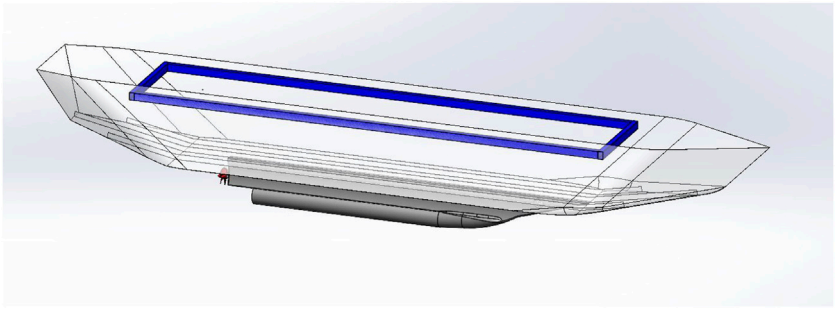

FIGURE 5
Integration of torsion box (blue).

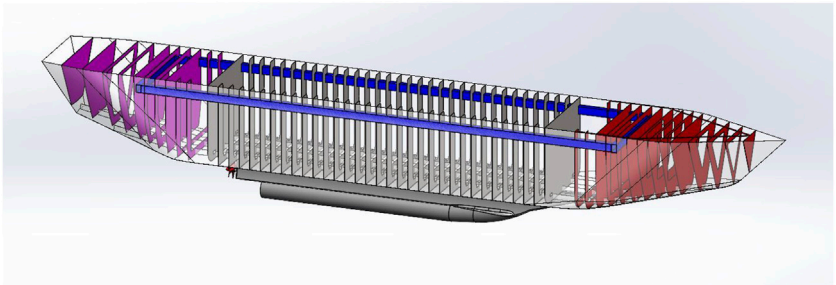

FIGURE 6
Integration of stiffeners, torsion box and transverse plates.

the centre of mass located 2.18 m below the deck. Stability analysis showed that the centre of gravity was located to the left of the metacentre when the ship tilted to the right, resulting in a stable vessel. The CAD model indicated that the keel had a surface area of 19.5 m^2. The function relating vessel velocity (V_B) and hull drag (F_{hull}) is expressed in Equation 18.

$$F_{hull} = 765.92V_B^{2.0538} \quad (18)$$

The structure inside the hull to house the masts is connected to the torsion box and to the lowest part of the hull (Figure 4 part 11). For the cargo hatch, a split folding plate mechanism was chosen (Figure 4 part 22).

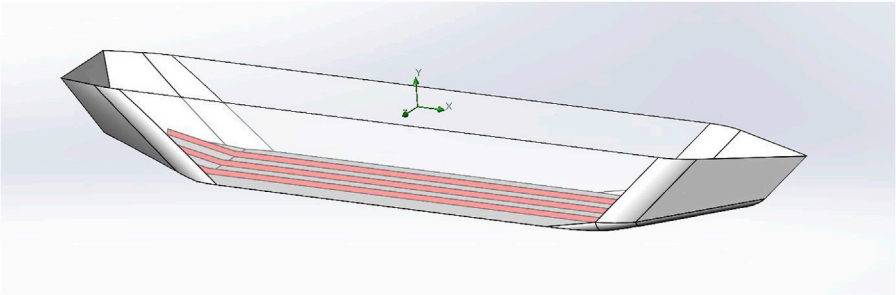

FIGURE 7
Longitudinal stiffeners on hull bottom (red).

TABLE 4 Corrected results longitudinal loads after integration of sails and keel.

Parameter	Unit	Quantity
Second moment of inertia (I_x)	[m^4]	0.0382
Maximum stress sagging	[MPa]	52.7
Maximum stress hogging	[MPa]	48.7

Sail design

To meet the requirements, the NACA 0015 has been chosen for the wing sail profile due to an L/D ratio of 77.9 at a Reynolds number of $1{\cdot}10^6$. The calculated Reynolds number for very low winds (0.6 m/s) is around $2.05{\cdot}10^5$. For extremely strong winds (32 m/s) it is around $1.10{\cdot}10^7$. For the steering flap the NACA 0009 was used. The iterations that have been done concerning the sail area concluded that for an average wind speed of 4 Bft., a velocity of 5 km/h is achievable for a wing sail area of around 184 m^2. The estimations of the velocity of the boat for different wind speeds and angles to the wind are seen in Figure 8.

For non-cambered NACA profiles, including the NACA 0015, the COE is at 25% from the chord length measured from the leading edge. The height of the COE is determined by the shape of the sail. Even though the shape of the chord length is not the same at every height, the ratios of the sail are made so, that the mast is always at 25% of the chord length. This makes the shape look like a windsurf sail, see Figure 4 part 2. The required sail area of 184 m^2 is divided into two smaller sails, with a surface area of 92 m^2. These sails have respectively a height, maximum width and maximum depth of 12.5 m, 9.33 m, and 1.4 m. The height of the COE and G respectively are at 5.73 m, and 4.43 m measured from the bottom of the sails. A steering flap (3) as shown in Figures 4, 9, attached at the back of the main sail, actuated by a linear actuator, is used to control the position of the sail. By initiating an angle with respect to the main sail, the steering flap creates a moment around the mast and therefore rotating the main sail to the desired angle of attack. The optimal angle of attack for the NACA 0015 aerofoil, relative to the wind, is 8° (Şahin and Acir, 2015).

The sails comprise of an outer shell and an inner material. According to GRANTA, Carbon-Fibre-Reinforced Polymers (CFRP) is the best option for the shell. It has excellent corrosion resistance properties, an average Young's modulus of 110 GPa, and a density of 1,600 kg/m^3. For the inner material, a honeycomb structure of the foam 'Divinycell H45′ was chosen. It has a density of 48 kg/m^3 and a compressive modulus of 45 MPa.

The counterweights, illustrated in Figure 4 part 18, were used to reduce the moment of the mast and weighed 850 kg. The combined mass of the steering flap, counterweights, and mast for the sails was estimated to be approximately 9,000 kg.

The fatigue strength resulted to be $\sigma_{\text{Fatigue}} = 2.17{\cdot}10^8$ MPa. Incorporating the safety margin of 3, the final dimensions of the mast are 0.5 m for the outer diameter of the mast, 0.442 m for the inner diameter of the mast. The final dimensions of the beam holding the steering flap are 0.12 m for the outer diameter and 0.037 m for the inner diameter.

The assumption was made that the strength of the chosen composite honeycomb core sandwich panel was sufficient to resist the forces acting on the sail using literature study (Bruffey and Shiu, 2016).

Systems for autonomy

In this section, the implementation of a Guidance, Navigation, and Control (GNC) scheme for the vessel is outlined. This involves linking the requirements stated in the design method section to the complete GNC framework, as illustrated in Figure 10. To fulfil the requirement of autonomous navigation between destinations, the implementation of a Global Navigation Satellite System (GNSS) is proposed. This system is essential for determining the vessel's precise location, and its optimal placement could be at the hull's tip or the mast's top to ensure clear signal reception. Path planning integrates classical methods for determining the fastest route, complemented by advanced algorithms for dynamic obstacles navigation, path re -planning, and collision avoidance.

Addressing the second and third requirements, which focus on the vessel's ability to communicate its position to other ships and identify the surrounding environment, a comprehensive situational awareness system within the navigation block is proposed (see Figure 10, left section). This system would merge data from an extensive array of exteroceptive sensors, including Long Waves

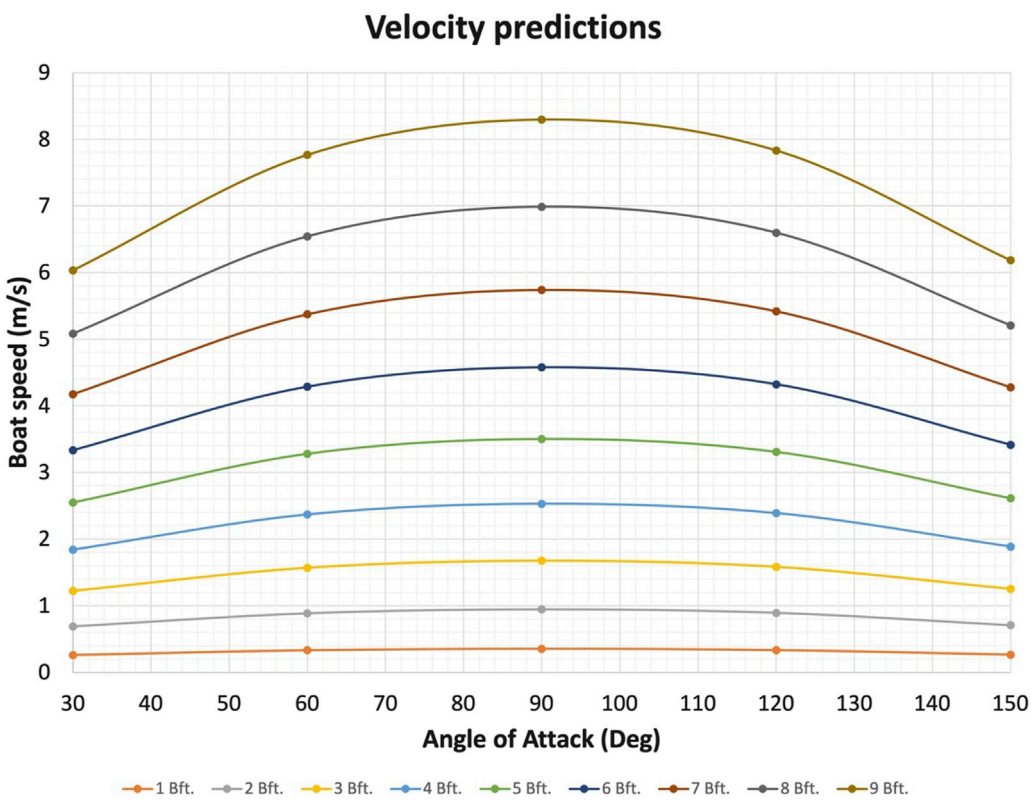

FIGURE 8
Velocity predictions of vessel.

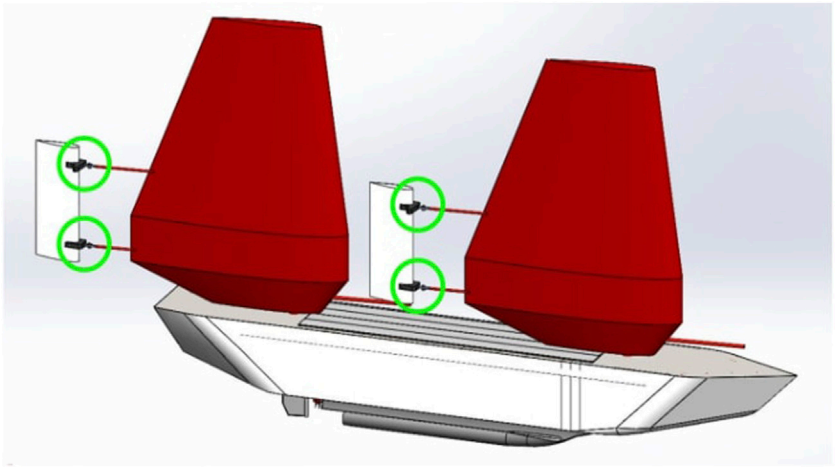

FIGURE 9
Visual representation of mast/sail assembly indicating the linear sail flap actuators in green.

Infrared (LWIR) cameras, radar, sonar, LiDAR, AIS, microphones, and echo sounders. These sensors, as detailed by Jokioinen et al. (2016), are designed to create a cohesive picture of the maritime environment, enabling the control strategy to effectively avoid obstacles.

The final requirement involves monitoring and maintaining the vessel's optimal sailing condition. Proprioceptive sensors are proposed for this purpose, measuring internal parameters such as ship's speed, accelerations, and the vessel's orientation in yaw, pitch, and roll. These measurements are vital for maintaining the optimal wind angle of attack and sailing condition. An Inertial Measurement Unit (IMU), which captures rotational states and accelerations, is central to this process. Additionally, an anemometer and wind vane would provide wind speed and direction data. Should sub-optimal

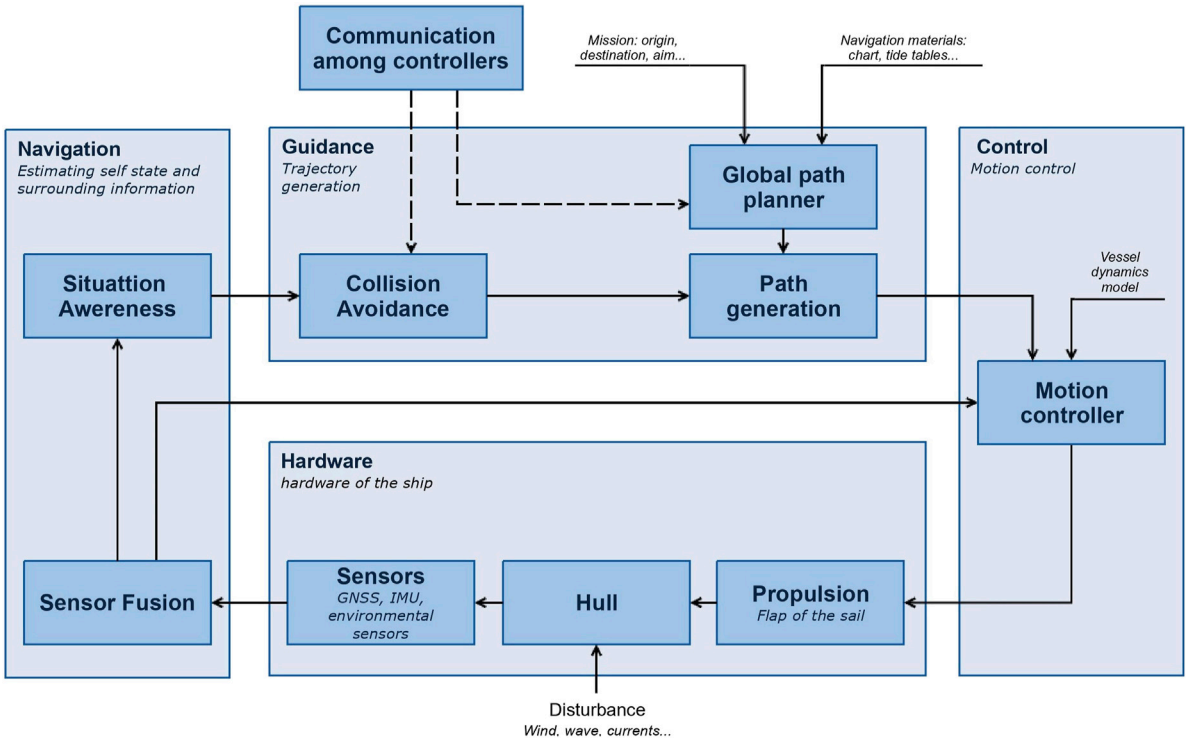

FIGURE 10
GNC of an autonomous single-container shipping solution, derived from Schiaretti, Chen and Negenborn (2017) with permission.

TABLE 5 Sensors to achieve autonomous navigation.

Sensor type	Data collected	Purpose/use in GNC system
GNSS Receiver	Global Position	Provides precise location data for navigation and path planning.
Radar	Obstacle Detection, Range	Detects and locates other vessels and large obstacles; used for collision avoidance and situational awareness.
Sonar	Underwater obstacles, Depth	Detects underwater objects and measures depth for safe navigation.
LiDAR	Obstacle detection, Distance, Shape	Provides detailed 3D mapping of the surrounding environment; used for obstacle detection and avoidance.
LWIR Camera	Thermal imagery	Used for detecting objects in low visibility conditions, such as at night or in fog.
AIS	Vessel information (position, speed, etc.)	Receives and sends information to/from other ships, aiding in collision avoidance and traffic management.
Echo Sounder	Water depth	Measures the depth beneath the vessel to prevent grounding in shallow waters.
Anemometer	Wind speed	Provides wind speed data, important for adjusting the vessel's course and sail settings.
Wind Vane	Wind direction	Measures wind direction, aiding in optimizing the vessel's orientation and angle of attack.
IMU	Orientation (yaw, pitch, roll), Acceleration	Monitors the vessel's orientation and movement, ensuring stability and optimal sailing conditions. Also used in the feedback loop for control adjustments.

conditions be detected by these sensors, the system would engage a linear actuator as part of a feedback loop, adjusting the sails until optimal sails angle-of-attack conditions are restored.

Integrating these components forms a robust GNC system, as depicted in Figures 4, 10, which provides an overview of all the necessary sensors (summarized in Table 5) and their suggested placements. This integration ensures that the vessel not only navigates efficiently and safely but also communicates effectively with other maritime entities and maintains its operational integrity under varying conditions.

Discussion

In this section, all results from the previous section will be discussed.

Hull design

Starting with the results of the different shapes of the 2D and 3D simulations. For both the front and the rear parts, a pointy shape resulted in the lowest drag force and relatively good sticking boundary layers around the hull. The rear of the final design eliminates nearly all vortexes, which has a positive effect on the drag. Only the fixation lines between the plates are rounded, as this improves local flow speeds significantly.

The first longitudinal strength analysis was needed to verify in an early stage to what extent the assumed model would be able to carry its own weight. Since this result was positive, it was relevant to continue with the next steps. The final maximum stress in the hull was 52.7 MPa. The maximum stress resulting from hydro-static pressure was 21.0 kPa. Most steels have a yield strength in the region of 200 MPa, and thus the hull will never yield in any static event. The displacement in the middle of a plate resulted in a maximum of 7.0 mm, which was deemed insignificant.

The justification for the reinforcements is as follows. The highest stresses occur on the bottom surface of the ship when it is sagging, which leads to compression on the upper part of the model. The risk of buckling, a concern for thin-walled plates, is eliminated through the integration of a torsion box. This strong member is welded to the entire length of the ship and contributes to the torsional stiffness, even though the research does not focus on dynamic loads. The transverse plates provide sufficient transverse stiffness against water pressure and distribute the mass of the container over the hull's bottom. The design of the tip and rear incorporates hollow and solid plates to create air pockets as specified in the requirements and accommodate components of the control systems. The hydrodynamic pressure on the bottom of the hull may cause inward bending of the plates, which could result in a harmonica-like effect. This is counteracted by the presence of three thin longitudinal stiffeners.

The results indicate a loaded immersion of 2.48 m and an empty submersion of 2.28 m. The stability analysis in the loaded condition demonstrated that the G is located on the lower side of the metacentre (M) when the ship tilts to the right, leading to a stable vessel up to a 90-degree. The stability analysis is not required to be extended to higher tilt angles, as the sails prevent the ship from rotating further. In the unloaded condition, the shift of the G towards the keel and the faster shift of the center of buoyancy towards the right when tilted to the right, confirms the stability of the vessel except in the rare case that the ship has capsized up to 90° and is located in completely flat waters as even the slightest waves would help the ship back to a stable position.

In accordance with the principles outlined in Fossati's book on Aero-Hydrodynamics (2009), the area of the keel should be 3.5% of the effective sail area for a 'cruising yacht'. Given that the dimensions and speed of the vessel in this research are similar to those of a cruising yacht, this assumption can be made. With an effective sail area of 184 m^2, the keel area should be at least 6.4 m^2. The results indicate a keel area of 19.5 m^2, which confirms that the keel is of sufficient size.

Sail design

The NACA 0015 aerofoil was selected for the design, despite not having the highest L/D coefficients at relevant Reynolds numbers. Cambered aerofoils were not considered due to the requirement of being able to utilize wind from any direction. While the NACA 0015 may not perform optimally at average wind speeds Reynolds numbers, it is among the top four aerofoils in terms of performance across all Reynolds numbers. Furthermore, it is one of the most widely researched and well-known NACA aerofoil profiles, making it an ideal choice for the theoretical design. The 184 m^2 NACA sails provide the vessel with enough thrust to reach the target speed of 1.39 m/s (5 km/h) from windspeeds of 3 Bft. and higher as depicted in Figure 8. Even the hull speed, or top speed, of 6.8 m/s can be reached during wind speeds of eight and 9 Bft.

The steering flaps that are used for trimming the main sails are eventually chosen above a torsion motor in the mast. A torsion motor would be efficient to trim the sails and it is widely used in small autonomous sailboats, but at this scale, it would cost too much force and thus energy to use as propelling force. The steering flaps, however, can trim the sails energy-efficiently (Silva et al., 2020). The NACA 009 profile was chosen, due to the smaller chord length resulting in lower Reynolds numbers.

To prevent that the sail causes the G of the complete vessel to shift to a point of instability, the required sail surface was evenly divided into two separate sails. This also offers the potential, if necessary, of rudderless sailing, or that the rudder and sail can be used cooperatively. This could be used as a backup if the rudder has a malfunction. Likewise, if one of the sails is malfunctioning the other sail would still provide sufficient propulsion. Another strong factor is that the COE is closer to the deck than with one large sail. This provides more stability with high wind speeds and downwind sailing, as the heeling moment is smaller. Although in this way more stability is provided for high wind speeds, to minimize the risk of failure, the vessel will be programmed to fully reef its sails if the wind speed passes 25 m/s. The division into two separate sails also offers practical advantages since symmetry can be maintained without obstructing the cargo hatch.

A foam honeycomb core sandwich panel structure was chosen to keep the total weight of the sails as low as possible to maintain as much compressive strength as possible, while having a fraction of the weight of solid foam. For the outside of the sail, CFRP is the material with the lowest density and the highest corresponding Young's modulus, which represents the ability to resist elastic deformation under stress. The only downside is, that it is a very expensive material. The total mass of the sails and mast was first estimated to be 7,000 kg but eventually turned out to be a fraction higher. This resulted in a G of the vessel that shifted a little bit up, but since there is more than enough slack, stability remains unaffected.

Systems for autonomy

In the results section, we detailed the control architecture and the sensor components necessary for achieving autonomous navigation in a maritime context. While this setup provides a comprehensive framework, further research is essential to fully realize and refine these autonomous systems.

The analysis highlighted the need for several distinct sensors, each with a unique role in establishing comprehensive situational awareness. The visual capabilities of the camera are critical for object identification, complemented by an IR camera's ability to work in

low-visibility conditions like fog or haze. LiDAR's contribution is invaluable, offering three-dimensional environmental mapping and enhancing prediction accuracy. The sonar sensor, with its underwater depth measurement, acts as a sub-sea detection tool. Additionally, AIS and Radar provide long-range measurement capabilities: AIS facilitates standard in positioning communication with other AIS-equipped vessels, while Radar offers independent, reliable detection.

Moreover, adaptation of this technologies, such as tailoring the performance of LiDAR to account for maritime conditions like ship movement, is a key area for further research. Simultaneously, the enhancement of existing maritime systems, such as intelligent interpretation of AIS data for autonomous situational awareness, presents another significant research field. It is important to note that this report does not investigate the details of the control strategy and the dynamic model of the vessel, which are equally crucial for autonomy, as these topics are beyond the current design scope.

Lastly, the consideration of active propulsion is essential, especially in scenarios where sails may not offer sufficient manoeuvrability, such as during mooring operations in ports. Our designs, as shown in Figure 4 (parts 8 and 11), incorporate the possibility of integrating active propulsion systems. This adaptability ensures that the vessel remains functional in various operational contexts, combining the efficiency of autonomous sailing with the precision of active propulsion when necessary.

Application

As stated in the introduction, the presented design could bring direct contributions to limitations in archipelagos around the world. A direct example can be imagined when looking at the island of Saba, a small island in the Dutch Antilles of the Caribbean which has a mere surface area of 13 km^2 and counts about 2,200 permanent inhabitants. Due to the island's limited maritime infrastructure, supplies of all kinds are brought only once a week on a fixed day by 50-m cargo ship 'Muttys Pride.' The ship houses 8 TEU and runs on diesel. The design presented in this study could provide a direct solution for this infrequent supply management with four autonomous deliveries a week, which would allow for a more balanced supply of goods while contributing to the sustainability goals of the area (Hofman et al., 2021).

Conclusion

This study has demonstrated that a predominantly passively propelled, autonomous vessel designed to carry a single container could be a viable solution to address the challenges posed by the increasing size of mega vessels. The proposed design achieves the target speed of 5 km/h under average sea conditions and presents a foundation for sustainable small-scale shipping, particularly in archipelagic regions where conventional large-scale maritime infrastructure is inadequate. While this research focused on the design of a hull and sail mechanism, it also acknowledges the seemingly utopian nature of substituting current large-scale maritime systems with such small-scale alternatives. However, in specific scenarios, such as isolated archipelagos, this design could offer a practical and sustainable complement to existing systems. Future research could further explore optimizing sensor technology, developing intelligent data interpretation systems, and integrating renewable energy sources, such as solar, wind, or wave energy, to ensure continuous operation and enhance sustainability. The sustainable autonomous single-container vessel concept not only provides a complementary solution to existing large-scale maritime transport systems but also offers a model that could inspire broader changes in global trade logistics. Although achieving a fully realized, small-scale autonomous shipping system may seem utopian, the continued exploration of this zero-emission approach is crucial in advancing toward a more sustainable and accessible maritime future, particularly for regions facing unique logistical challenges.

Data availability statement

The original contributions presented in the study are included in the article/supplementary material, further inquiries can be directed to the corresponding author.

Author contributions

JH: Writing–original draft, Writing–review and editing. PS: Writing–original draft. JT: Writing–original draft. TF: Writing–original draft. WS: Writing–original draft. YN: Conceptualization, Supervision, Writing–review and editing. VG: Methodology, Supervision, Writing–original draft, Writing–review and editing. JJ: Methodology, Supervision, Writing–original draft, Writing–review and editing.

Funding

The author(s) declare that no financial support was received for the research, authorship, and/or publication of this article.

Conflict of interest

Author YN was employed by company Technology of Future Utopia (TOFU).

The remaining authors declare that the research was conducted in the absence of any commercial or financial relationships that could be construed as a potential conflict of interest.

Publisher's note

References

ANSYS, Inc (2023). *Ansys GRANTA EduPack software*. Cambridge, UK. Available at: www.ansys.com/materials.

Anthierens, C., Pauly, E., and Jeay, F. (2013). MARIUS: a sailbot for sea-sailing. *Int. Robot. Sail. Conf.*, 3–12. doi:10.1007/978-3-319-02276-5_1

Archer, C. L., and Jacobson, M. Z. (2005). Evaluation of global wind power. *J. Geophys. Res.* 110, D12110. doi:10.1029/2004JD005462

Blanke, M., Henriques, M., and Bang, J. (2017). *A pre-analysis on autonomous ships*. Kongens Lyngby, Denmark: Technical University of Denmark.

Boeijen, A. van, and Daalhuizen, J. (2014). *Delft design guide*. Amsterdam, Netherlands: Bis Publishers.

Bruffey, N., and Shiu, W. (2016) "Predicting flexural strength of composite honeycomb sandwich panels using mechanical models of face sheet compressive strength,". California Polytechnic State University. Bachelor thesis.

Castanho, R. A., Behradfar, A., Vulevic, A., and Gomez, J. M. N. (2020). Analyzing transportation sustainability in the canary islands archipelago. *Infrastructures* 5 (58), 58. doi:10.3390/infrastructures5070058

Castanho, R. A., Gomez, J. M. N., Vulevic, A., Behradfar, A., and Couto, G. (2021). Assessing transportation patterns in the Azores archipelago. *Infrastructures* 6 (10), 10. doi:10.3390/infrastructures6010010

Engineers Edge (2021). *Rectangular plate uniform load simply supported equations and calculator*. Available at: https://www.engineersedge.com/material_science/rectangular_plate_uniform_load_13643.htm (Accessed June 29, 2021).

Fossati, F. (2009). *Aero-hydrodynamics and the performance of sailing yachts: the science behind sailing yachts and their design*. London, United Kingdom: Bloomsbury.

Gentemann, C. L., Scott, J. P., Mazzini, P. L. F., Pianca, C., Akella, S., Minnett, P. J., et al. (2020). Saildrone: adaptively sampling the marine environment. *Bull. Am. Meteorological Soc.* 101 (6), E744–E762. doi:10.1175/BAMS-D-19-0015.1

Ghani, M. H., Hole, L. R., Fer, I., Kourafalou, V. H., Wienders, N., Kang, H., et al. (2014). The SailBuoy remotely-controlled unmanned vessel: measurements of near surface temperature, salinity and oxygen concentration in the Northern Gulf of Mexico. *Methods Oceanogr.* 10, 104–121. doi:10.1016/j.mio.2014.08.001

Heo, J., Kim, J., and Kwon, Y. (2017). Analysis of design directions for unmanned surface vehicles (USVs). *J. Comput. Commun.* 5, 92–100. doi:10.4236/jcc.2017.57010

Hofman, C. L., Stancioff, C. E., Richards, A., Auguiste, I. N., Sutherland, A., and Hoogland, M. L. P. (2021). Resilient caribbean communities: a long-term perspective on sustainability and social adaptability to natural hazards in the lesser Antilles. *Sustainability* 13 (9807), 9807. doi:10.3390/su13179807

ITF (2015). The impact of mega ships. *Int. Transp. Forum*, 107.

Jokioinen, E., Poikonen, J., Hyvönen, M., Kolu, A., Jokela, T., Tissari, J., et al. (2016). Remote and autonomous ships: the next steps. *Rolls-Royce plc*.

Keuning, J. A. (2015). *Introductie minor zeiljachten: mt-mi-105-15*. Delft, Netherlands: TU Delft.

King, M. (2017). *Asia-europe trade set for 24,000 TEU ships from 2019*. Lloyd's Loading List. Available at: https://www.lloydsloadinglist.com/freight-directory/news/Asia-Europe-trade-set-for-24000-teu-ships-from-2019/70733.htm#.ZA84Ny-iFqt (Accessed November 13, 2017).

Makkonen, T., Salonen, M., and Kajander, S. (2013). Island accessibility challenges: rural transport in the Finnish archipelago. *EJTIR* 13 (4), 274–290. doi:10.18757/ejtir.2013.13.4.3005

Negenborn, R. R., Goerlandt, F., Johansen, T. A., Slaets, P., Valdez Banda, O. A., Vanelslander, T., et al. (2023). Autonomous ships are on the horizon: here's what we need to know. *Nature* 615, 30–33. doi:10.1038/d41586-023-00557-5

Okumoto, Y., Takeda, Y., Mano, M., and Okada, T. (2009). *Design of ship hull structures: a practical guide for engineers*. Springer.

Ralahalu, K. A., and Jinca, M. Y. (2013). The development of Indonesia archipelago transportation. *Int. Refereed J. Eng. Sci. (IRJES)* 2 (9), 12–18.

Rødseth, O. J., and Nordahl, H. (2017). "Norwegian forum for autonomous ships," in *Definitions for autonomous merchant ships*. Available at: https://www.researchgate.net/profile/Ornulf-Rodseth-2/publication/348716003_Definitions_for_Autonomous_Merchant_Ships/links/600c5a50a6fdccdcb8770a2b/Definitions-for-Autonomous-Merchant-Ships.pdf (Accessed August 27, 2024).

Russon, M. (2021). The cost of the suez canal blockage. *BBC News*. Available at: https://www.bbc.com/news/business-56559073 (Accessed March 29, 2021).

Şahin, İ., and Acir, A. (2015). Numerical and experimental investigations of lift and drag performances of NACA 0015 wind turbine airfoil. *Int. J. Mater. Mech. Manuf.* 3 (1), 22–25. doi:10.7763/IJMMM.2015.V3.159

Santos, D. H., and Gonçalves, L. M. G. (2020). Performance evaluation of propulsion control techniques for autonomous sailboat. *Lat. Am. Robot. Symp. (LARS)*. doi:10.1109/LARS/SBR/WRE51543.2020.9307155

Schiaretti, M., Chen, L., and Negenborn, R. R. (2017). "Survey on autonomous surface vessels: Part I - a new detailed definition of autonomy levels," in *Computational logistics, LNCS 10572*. Editors T. Bektaş, S. Coniglio, and A. Martinez-Sykora (Springer).

Silva, M. F., Malheiro, B., Guedes, P., and Ferreira, P. (2020). "Airfoil selection and wingsail design for an autonomous sailboat," in Robot 2019: Fourth Iberian Robotics Conference. ROBOT 2019. AISC (Nature Switzerland: Springer), 305–316.

Sirimanne, S. N., and Hoffmann, J. (2020). *Review of maritime transport 2020*. New York, United States: United Nations.

Tretow, C. (2017). *Design of a free-rotating wing sail for an autonomous sailboat*. Stockholm, Sweden: KTH Royal Institute of Technology.

Weber, H., Wiek, A., and Lang, D. J. (2019). Sustainability entrepreneurship to address large distances in international food supply. *Bus. Strategy Dev.* 3, 318–331. doi:10.1002/bsd2.97

Zhang, Q., Zhu, Y., Gao, X., Wu, Y., and Hutchinson, C. (2020). Training high-strength aluminum alloys to withstand fatigue. *Nat. Commun.* 11, 5198. doi:10.1038/s41467-020-19071-7